Europace (2015) **17**, 1282–1288
doi:10.1093/europace/euu339

Validation of the mapping accuracy of a novel non-invasive epicardial and endocardial electrophysiology system

Amiran S. Revishvili[1], Erik Wissner[2]*, Dmitry S. Lebedev[3], Christine Lemes[2], Sebastian Deiss[2], Andreaas Metzner[2], Vitaly V. Kalinin[1], Oleg V. Sopov[1], Eugeny Z. Labartkava[1], Alexander V. Kalinin[4], Michail Chmelevsky[3], Stephan V. Zubarev[3], Maria K. Chaykovskaya[5], Mikhail G. Tsiklauri[5], and Karl-Heinz Kuck[2]

[1]Bakoulev Scientific Center for Cardiovascular Surgery of the Russian Academy of Science, Moscow, Russia; [2]Stereotaxis Laboratory, Asklepios Klinik St Georg, II. Medizinische Abteilung, Lohmühlenstraße 5, Hamburg 20099, Germany; [3]Federal Almazov Medical Research Center, St Petersburg, Russia; [4]Institute for Information Transmission Problems of the Russian Academy of Science, Moscow, Russia; and [5]EP Solutions SA, Yverdon-les-Bains, Switzerland

Received 12 July 2014; accepted after revision 3 November 2014; online publish-ahead-of-print 2 February 2015

Aims Use of a non-invasive electrocardiographic mapping system may aid in rapid diagnosis of atrial or ventricular arrhythmias or the detection of ventricular dyssynchrony. The aim of the present study was to validate the mapping accuracy of a novel non-invasive epi- and endocardial electrophysiology system (NEEES).

Methods and results Patients underwent pre-procedural computed tomography or magnetic resonance imaging of the heart and torso. Radiographic data were merged with the data obtained from the NEEES during pacing from implanted pacemaker leads or pacing from endocardial sites using an electroanatomical mapping system (CARTO 3, Biosense Webster). The earliest activation as denoted on the NEEES three-dimensional heart model was compared with the true anatomic location of the tip of the pacemaker lead or the annotated pacing site on the CARTO 3 map. Twenty-nine patients [mean age: 62 $\pm$ 11 years, 6/29 (11%) female, 21/29 (72%) with ischaemic cardiomyopathy] were enrolled into the pacemaker verification group. The mean distance from the non-invasively predicted pacing site to the anatomic reference site was 10.8 $\pm$ 5.4 mm for the right atrium, 7.7 $\pm$ 5.8 mm for the right ventricle, and 7.9 $\pm$ 5.7 mm for the left ventricle activated via the coronary sinus lead. Five patients [mean age 65 $\pm$ 4 years, 2 (33%) females] underwent CARTO 3 verification study. The mean distance between non-invasively reconstructed pacing site and the reference pacing site was 7.4 $\pm$ 2.7 mm for the right atrium, 6.9 $\pm$ 2.3 mm for the left atrium, 6.5 $\pm$ 2.1 mm for the right ventricle, and 6.4 $\pm$ 2.2 for the left ventricle, respectively.

Conclusion The novel NEEES was able to correctly identify the site of pacing from various endo- and epicardial sites with high accuracy.

Keywords Non-invasive mapping system • Endocardial mapping • Epicardial mapping • Arrhythmias

Introduction

Due to the inherent limitations of the 12-lead surface ECG to provide accurate information on the precise location and activation sequence of cardiac arrhythmias within the human heart, non-invasive electrocardiographic imaging (ECGI) was developed.[1–3] Electrocardiographic imaging is based on non-invasive numerical reconstruction of cardiac activation from unipolar body surface potentials combined

* Corresponding author. Tel: +49 40 1818 85 4488; fax: +49 40 1818 85 2977, *E-mail address*: e.wissner@asklepios.com

What's new?

- A novel non-invasive epi- and endocardial electrophysiology system (NEEES) was able to identify with high accuracy the site of pacing from different endo- and epicardial sites.
- Use of the novel NEEES may facilitate accurate non-invasive identification of focal atrial or ventricular arrhythmias and proper delineation of the re-entry wavefront.

with data on anatomy and position of the body surface electrodes from CT or MRI. The use of ECGI may facilitate rapid non-invasive diagnosis of atrial or ventricular arrhythmias or the detection of ventricular dyssynchrony.[4–9]

Early ECGI systems allowed non-invasive mapping of the epicardial surface. Recently, non-invasive mapping of both epi- and endocardial surfaces applying novel numerical algorithms was reported.[10–12] The aim of the present study was to validate the mapping accuracy of a novel non-invasive epi- and endocardial electrophysiology system (NEEES).

Methods

Patient preparation and radiographic imaging

Prior to the electrophysiology study, a maximum of 224 unipolar body surface mapping electrodes compatible with MRI or CT imaging were placed onto the patient's torso (*Figure 1*), followed by same-day ECG-gated contrast MRI (Magnetom Avanto, 1.5 T, Siemens AG) or CT (Somatom Definition 128, Siemens AG) scanning of the heart and thorax. In the electrophysiology laboratory, custom-built MRI-compatible body surface mapping electrodes were connected to the multichannel ECG amplifier as part of the NEEES (EP Solutions SA).

During CT imaging two scans were performed in a craniocaudal direction. The first scan examined the anatomy of the torso, including all body surface electrodes applied to the patient's upper body. The scan of the torso was processed using a slice thickness of 5 mm and reconstruction steps of 3 mm. The high-resolution ECG-gated scan of the heart was performed thereafter using automated intravenous injection of a non-ionic contrast bolus to a maximum of 2 mL/kg body weight during breath hold. Data reconstruction was performed using a slice thickness of 3 mm and reconstruction steps of 1.5 mm.

Magnetic resonance imaging scanning followed the same general principles applied to CT imaging with regard to resolution, scanning direction, patient position, and breath hold. A 'localizer scan' was performed initially to determine upper and lower margins of the torso such as to keep all body surface electrodes in the field of view. Between 7.5 and 20 mL of gadolinium-based contrast agent was injected, maintaining optimal contrasting during the initial 5–15 min following injection, depending on the agent used. The main scanning series was completed without ECG-gating utilizing the scanner sequences that allowed saving data in the form of axial section sets (slices) to implement volume reconstruction. The slice thickness did not exceed 3–5 mm.

Torso and heart volume reconstruction

Radiographic data imported in DICOM format and coordinates of all unipolar ECG electrodes were automatically processed by the NEEES, to render a realistic three-dimensional reconstruction of the torso geometry and surface electrodes positions (*Figure 1*). The three-dimensional heart model was plotted semi-automatically and segmentation optimized using a three-dimensional editor program as part of the NEEES. A tailored approach to three-dimensional heart and torso reconstruction has been described previously.[13,14] In the current study, a similar technique was used except for the difference in custom-built body surface mapping electrodes utilized.

Torso and three-dimensional heart model generation

Following heart and torso segmentation and volume reconstruction, the surfaces of the torso and cardiac chambers were triangulated and polygonal meshes constructed. The surface triangulation procedure included construction of the primary surface mesh using the marching cubes method.[15] Smoothing and attenuation was performed using the boundary correction method.[16] The three-dimensional tetrahedral mesh was constructed using the advancing front approach.[17]

Rendering of non-invasive epi- and endocardial maps

In order to display cardiac activation at a given point during the cardiac cycle, multichannel ECG recordings 15–30 s in duration were logged

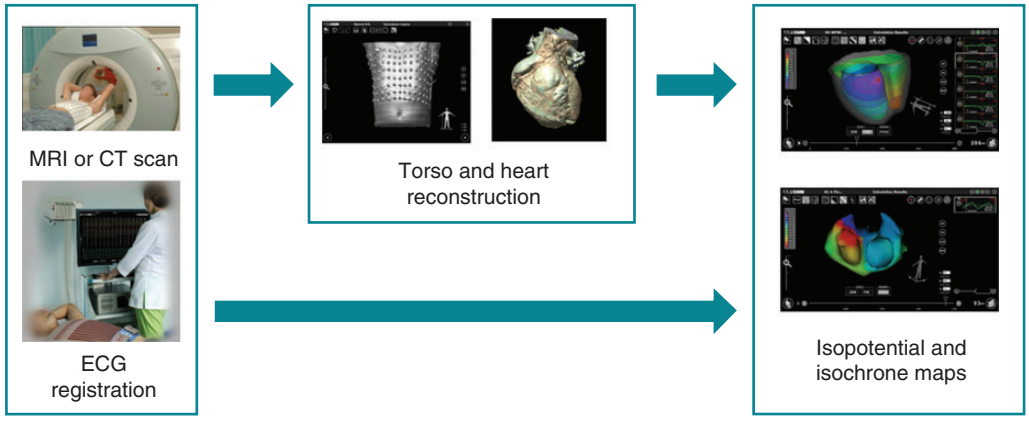

Figure 1 Non-invasive endo- and epicardial electrophysiology study procedure (see text for details).

and exported into the NEEES. The imported ECG files were processed by NEEES inverse problem solution software in combination with heart and torso anatomy data. The resulting endo- and epicardial isopotential maps were reconstructed on the three-dimensional heart model and displayed as individual frames or as activation movies (*Figure 2A* and *B*). Isopotential maps were analysed to determine the earliest activation zone, i.e. the potential minimum during early depolarization.

Validating the accuracy of the non-invasive epi- and endocardial electrophysiology system

In order to assess the accuracy of the NEEES, a two-step approach was used.

During step 1, patients scheduled in the device clinic for regular check-up and device optimization were included and stimulation from the atrial or ventricular pacemaker leads was performed at a rate of 80 b.p.m. In a subgroup of patients, pacing was completed during breath holding in order to assess the impact of breathing on the accuracy of non-invasive reconstruction. During pacing, multichannel ECG recordings were logged and subsequently imported into the NEEES. A minimum number of six consecutive pacing stimuli were analysed in order to average the impact of potential confounding factors such as ECG signal noise.

The earliest activation as denoted on the NEEES three-dimensional heart model was compared with the true anatomic location of the pacing electrode. The precise position of the pacemaker lead was visualized in the NEEES using the same CT or MRI data to reconstruct the three-dimensional cardiac model and applying a semi-transparent myocardial mode (*Figure 3*). The position of the pacing electrode was annotated and transferred onto the three-dimensional non-invasive cardiac surface map (*Figure 4A*). Next, the site of earliest activation on the non-invasive cardiac surface map was marked and the distance between both was measured to validate the accuracy of the NEEES (*Figure 4B*).

In order to assess for data reproducibility, analysis was performed for each patient at least six times per pacing site.

During step 2, the NEEES was used in concert with a three-dimensional electroanatomical mapping system (CARTO 3, Biosense Webster Inc.) in patients referred for catheter ablation of atrial fibrillation. Magnetic resonance imaging scanning was used in two of five (40%) patients. A point-by-point electroanatomical map was created followed by pacing from the distal tip of the ablation catheter (Thermocool Navistar, Biosense Webster Inc.) during sinus rhythm at a rate of 80–90 b.p.m. either at the onset or at the end of the ablation procedure. The operator selected each pacing site and annotated its position on the three-dimensional electroanatomical map (*Figure 5*), while those team members acquiring the NEEES body surface ECG and processing the NEEES non-invasive results were blinded with regards to the location of the individual pacing sites. Analysis of the non-invasively reconstructed isopotential maps allowed locating the earliest site of cardiac activation. This site was termed the reconstructed pacing site and marked on the MRI or CT-based three-dimensional heart model (*Figure 5*).

Following completion of the procedure, each electroanatomical CARTO map was exported as a polygonal mesh, including all marked reference pacing site coordinates and processed along with data from the NEEES containing the MRI or CT-based three-dimensional heart model as a polygonal mesh and all annotated reconstructed pacing sites.

The three-dimensional heart models generated by the CARTO system and the NEEES were merged utilizing a special software integrated into the NEEES (*Figure 5*). If the volume of the space between the superimposed three-dimensional CARTO and NEEES mesh surfaces exceeded 10% of the volume of the CARTO map, the merged maps were exempt from further data analysis. The nearest point on the NEEES mesh model (ref PS) was determined for each CARTO pacing site (CARTO PS) previously marked on the CARTO mesh model (see Supplementary material online, *Figure S1*).

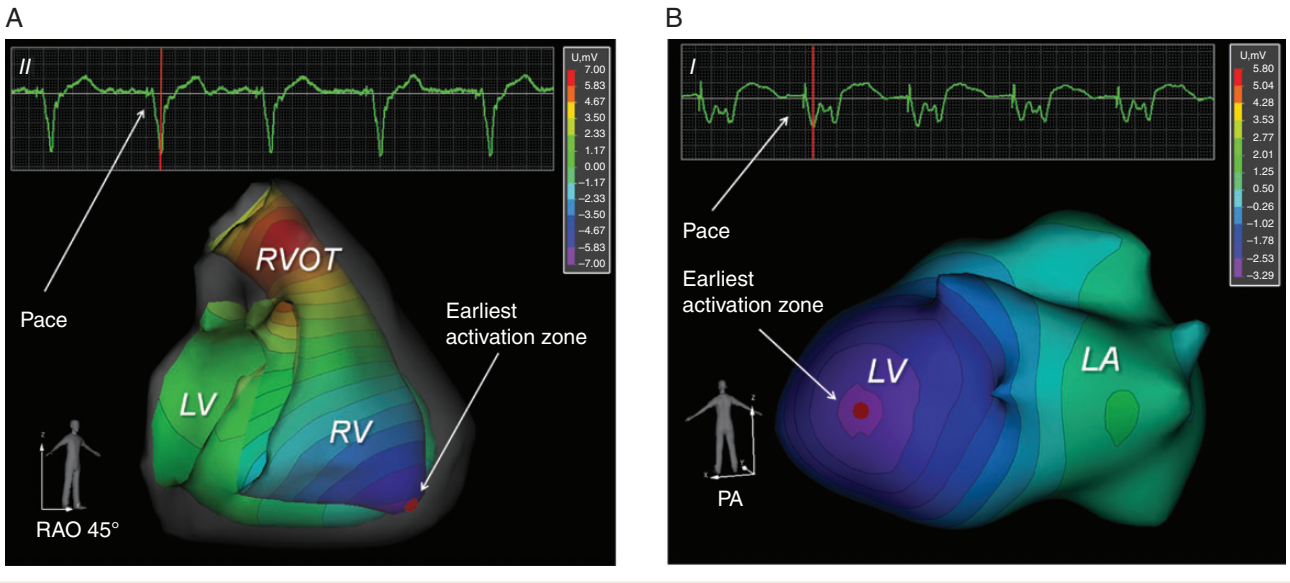

Figure 2 (*A*) Non-invasively reconstructed endocardial isopotential map with earliest activation zone (first negative potential breakthrough) at the region of the right ventricular apex during pacing from the right ventrical apex in a patient with a cardiac resynchronization device. Colour coding from negative (purple) to positive (red) isopotential. See also Supplementary material online, *Video S1*. (*B*) Non-invasively reconstructed epicardial isopotential map with earliest activation zone (first negative potential breakthrough) along the posterolateral left ventricular wall during pacing from the posterolateral wall of the left ventricle in a patient with a cardiac resynchronization device. Colour coding from negative (purple) to positive (red) isopotential. See also Supplementary material online, *Video S2*.

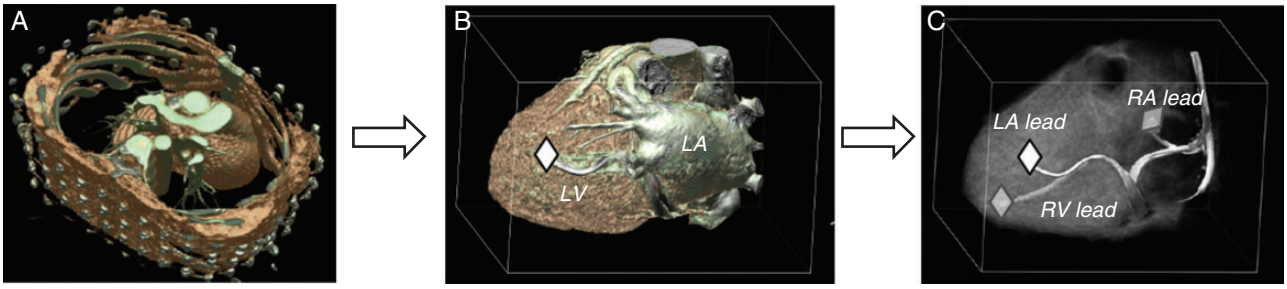

Figure 3 Computed tomography-based volume rendering, three-dimensional heart reconstruction, and marking of distal tip of the coronary sinus, right atrial, and right ventricular pacemaker lead. (*A*) Computed tomography of torso and heart, volume rendering. (*B*) Three-dimensional heart reconstruction, volume rendering after segmentation using the non-transparent mode (distal tip of coronary sinus lead is marked). (*C*) Three-dimensional heart reconstruction, volume rendering after segmentation using the semi-transparent myocardial mode. This mode allows simultaneous visualization of the epicardial coronary sinus lead and the endocardial right atrial and ventricular pacing leads.

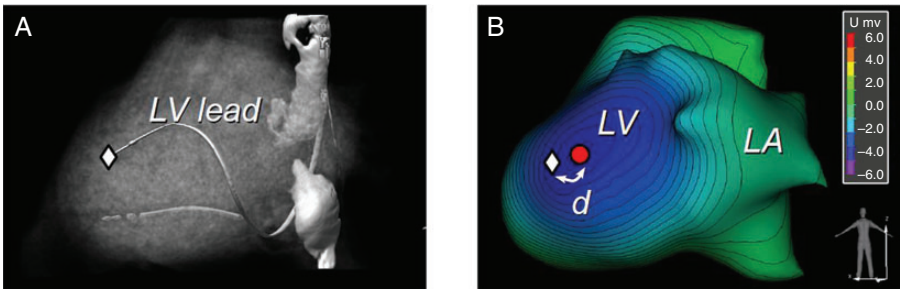

Figure 4 Non-invasive reconstruction of an epicardial pacing site. (*A*) Three-dimensional heart reconstruction, volume rendering after segmentation using the semi-transparent myocardial mode. Position of the tip of the coronary sinus lead is marked with a white diamond. (*B*) Non-invasive reconstruction of an epicardial isopotential map superimposed on the three-dimensional heart model demonstrating earliest activation along the distal tip of the coronary sinus lead. The anatomical position of the distal tip of the coronary sinus lead is marked with a white diamond, reconstructed pacing site is marked by red dot.

Analysis was based on ref PS in order to compensate for the insufficient specificity of the CARTO mesh model constructed from a limited number of mapping points compared with the high-resolution MRI or CT-derived heart models. The distance between ref PS and reconstructed pacing sites on the NEEES mesh model was measured using the 'ruler' function integrated with the NEEES software (see Supplementary material online, *Figure S1*).

For each pacing site, at least six consecutive pacing stimuli were analysed in order to average the influence of random factors such as patient breathing or ECG signal noise.

The validation study in patients with implanted devices was performed at Almazov Federal Research Medical Center in St Petersburg, Russia. The validation study using the CARTO 3 mapping system was performed at Asklepios Klinik St Georg in Hamburg, Germany and at Bakoulev Research Center for Cardiovascular Surgery in Moscow, Russia. All patients provided written informed consent. The local ethics review committees approved the study.

Statistical analysis

During statistical data processing, the mean distances between reference sites and reconstructed pacing sites, as well as the standard deviations from the mean distances were calculated for all pacing sites and cardiac cycles. The results are shown in the corresponding tables as mean distances ± standard deviation and are expressed as absolute values. Statistical analysis of the data was performed with SciPy, version 0.14.0 for Windows. The Student's *t*-test (unpaired) was used to evaluate mean differences between statistical data groups.

Results

Verification of pacing site using pacing from implanted pacing leads

Twenty-nine patients (23 men, mean age 62 ± 11 years) with previously implanted devices seen for regular check-up at the pacemaker clinic were enrolled. Twenty-one of 29 (72%) patients had a history of ischaemic cardiomyopathy, 7 of 29 (24%) patients had a history of dilated cardiomyopathy, and 1 of 29 (4%) had a history of restrictive cardiomyopathy. The type of implanted device, predominant rhythm at the time of study, and type of underlying conduction disturbance are summarized in Supplementary material online, *Table S1*. Pacing was performed from a total of 76 pacing sites: 21 in the right

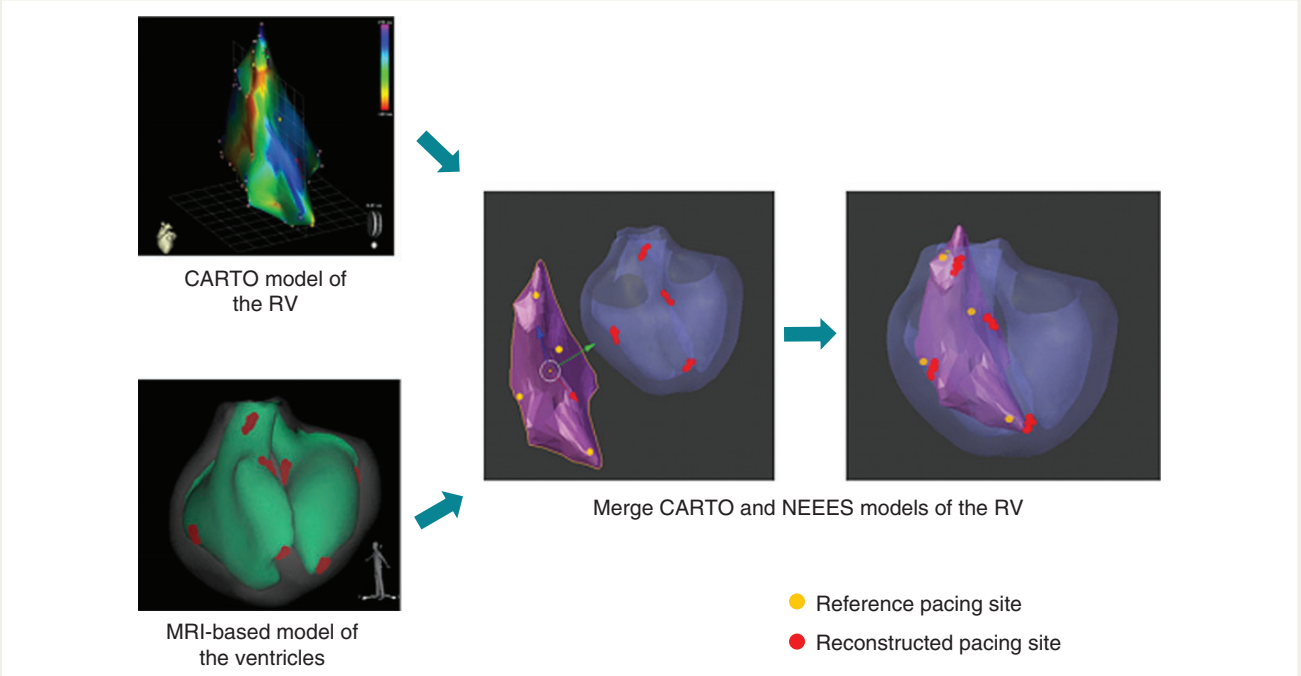

Figure 5 Merging the invasive three-dimensional electroanatomical map (CARTO 3, Biosense Webster Inc.) with the MRI-based non-invasively reconstructed model using the NEEES. Non-invasively reconstructed pacing sites with earliest activation are annotated in red.

Table 1 Accuracy according to paced cardiac chamber and number of pacing attempts analysed in implanted device study cohort

Heart chamber	RA, endocardium (*N* = 126)	RV, endocardium (*N* = 174)	LV, epicardium (*N* = 156)	RA + RV + LV (*N* = 456)
Mean ± SD (mm)	10.8 ± 5.4	7.7 ± 5.8	7.9 ± 5.7	8.6 ± 5.8

Mean distance between reference pacing site and reconstructed pacing site and standard deviation for *N* pacing events.
RA, right atrium; RV, right ventricle; LV, left ventricle.

atrium, 29 in the right ventricle, and 26 in the left ventricle through the coronary sinus, respectively. The different pacing lead positions are detailed in Supplementary material online, *Tables S2* and *S3*.

The mean distance from the non-invasively predicted pacing site to the anatomic reference site was 10.8 ± 5.4 mm for the right atrium, 7.7 ± 5.8 mm for the right ventricle, and 7.9 ± 5.7 mm for the left ventricle activated via the coronary sinus lead (*Table 1*). No significant difference in accuracy was found for the left vs. right ventricular sites ($P = 0.815$), while the difference in accuracy was significant comparing ventricular and atrial sites ($P < 0.001$).

The influence of breathing on the accuracy of non-invasive reconstruction was studied in a subgroup of six patients. Breath hold during inspiration (see Supplementary material online, *Figure S2*) as compared with free breathing or breath hold on expiration resulted in highest accuracy, that is, smallest difference in the mean distance from non-invasively predicted pacing site to reference pacing site (*Table 2*).

Verification of pacing site using a three-dimensional electroanatomical mapping system

Five patients (four with paroxysmal and one with persistent atrial fibrillation, four males, mean age 65 ± 4 years) referred for pulmonary vein isolation aided by three-dimensional electroanatomical mapping underwent electrical stimulation from a total of 412 different intracardiac positions. The mean distance between non-invasively reconstructed pacing site and the reference pacing site was 7.4 ± 2.7 mm for the right atrium, 6.9 ± 2.3 mm for the left atrium, 6.5 ± 2.1 mm for the right ventricle, and 6.4 ± 2.2 mm for the left ventricle, respectively (*Table 3*). There was a statistically significant difference in accuracy comparing the mean distance for both ventricles vs. the left and right atria ($P = 0.004$), while no statistically significant difference in accuracy was found for the left vs. right ventricle ($P = 0.864$) or left vs. right atrium ($P = 0.143$).

Table 2 Effect of breathing on the accuracy of the NEEES

Heart chamber	RA ($N = 24$)	RV ($N = 36$)	LV ($N = 36$)	RA + RV + LV ($N = 96$)
Spontaneous breathing, mean ± SD (mm)	8.0 ± 1.8	6.3 ± 1.8	6.4 ± 1.5	6.8 ± 1.9 ($P < 0.001$ vs. inspiration and expiration)
Inspiration breath hold, mean ± SD (mm)	5.9 ± 1.3	4.7 ± 1.3	5.9 ± 1.6	5.5 ± 1.6 ($P < 0.001$ vs. spontaneous breathing and expiration)
Expiration breath hold, mean ± SD (mm)	9.5 ± 1.9	8.1 ± 1.7	8.5 ± 1.1	8.6 ± 1.6 ($P < 0.001$ vs. spontaneous breathing and inspiration)

Pacing during spontaneous breathing and during breath hold on inspiration and expiration. Mean distance between reference pacing site and reconstructed pacing site and standard deviation for *N* pacing events.
RA, right atrium; RV, right ventricle; LV, left ventricle.

Table 3 Results for the CARTO pacing study according to anatomical site paced

Heart chamber	RA ($N = 92$)	LA ($N = 167$)	RV ($N = 61$)	LV ($N = 92$)	RA + LA + RV + LV ($N = 412$)
Mean distance ± SD (mm)	7.4 ± 2.7	6.9 ± 2.3	6.5 ± 2.1	6.4 ± 2.2	6.8 ± 2.4

Mean distance between reference pacing site and reconstructed pacing site and standard deviation for *N* pacing events.
RA, right atrium; LA, left atrium; RV, right ventricle; LV, left ventricle; SD, standard deviation.

Discussion

The present study demonstrates that non-invasive reconstruction of individual pacing sites using a novel NEEES is feasible and accurate. The cardiac structure from which stimulation was performed was recognized correctly in all cases.

While stimulation from the permanent coronary sinus lead results in early activation of the epicardial layer of the ventricular myocardium, pacing from the right atrial and right ventricular lead causes the activation front to spread from endo- to epicardium. Applying a similar principle than previously described for non-invasive electrocardiographic imaging systems for obtaining endocardial electrophysiological data, the NEEES adds the option to simultaneously map the endo- and epicardial surfaces and was equally effective in delineating epi- or endocardial pacing sites.

The current results are in line with a study by Cucculich *et al.* assessing the accuracy of a non-invasive electrocardiographic imaging system in patients with atrial fibrillation. Spatial accuracy within the left atrium was 6.3 ± 3.9 mm compared with a three-dimensional electroanatomical mapping system.[8] Oster *et al.*[1] analysed the accuracy of a non-invasive electrocardiographic imaging system in the ventricle reporting an accuracy of 2–10 mm. The present study indicates that respiration influences the accuracy of the non-invasive reconstructed pacing site location. Respiration may result in cyclic changes of the anatomical relationship between heart and torso and may alter the electrical conductivity of the lungs. The highest accuracy for reconstructed pacing sites was observed during breath hold on inspiration. This may simply be explained by the fact that pre-procedural CT imaging is also routinely being performed during breath hold on inspiration.

Compared with other available non-invasive mapping systems relying merely on epicardial surface information, the NEEES is capable of mapping both the endo- and epicardial surface. Extrapolating the findings from the current study into clinical practice, the use of the NEEES may facilitate accurate non-invasive identification of focal atrial or endo- or epicardial ventricular arrhythmias and proper delineation of the re-entry wavefront. Furthermore, the NEEES may aid in non-invasive optimization of resynchronization therapy.

In addition to its non-invasive nature, the NEEES offers the ability to simultaneously reconstruct activation patterns of all four cardiac chambers during a single cardiac cycle.

Limitations

Comparing the NEEES to the CARTO electroanatomical mapping system may have introduced a source of error due to the inherent differences in the geometries created. However, the use of the CARTO system was advantageous, in that pacing could be performed from various atrial and ventricular sites, while statistical processing compensated to some extent for geometrical differences. In contrast, the stimulation protocol utilizing implanted pacemaker leads to verify the accuracy of the NEEES permitted only a limited number of pacing locations to be selected in each patient. However, the exact position of each pacing lead could be integrated into the NEEES with high accuracy using the CT data set. While team members acquiring and processing the NEEES data were blinded during the validation study using the CARTO three electroanatomical mapping system, this was not the case for the validation study using implanted devices. The latter may have introduced a source of bias in the validation of the NEEES.

Conclusion

The novel NEEES was able to correctly identify the site of pacing from various endo- and epicardial sites with high accuracy. Future studies are indicated to assess the feasibility of the NEEES to correctly diagnose the origin of focal or re-entry arrhythmia within the human heart.

Supplementary material

Supplementary material is available at Europace online.

Conflict of interest: A.S.R., V.V.K., and M.G.T. are cofounders of EP Solutions SA, Yverdon-les-Bains, Switzerland. E.W. is consultant to EP Solutions. M.K.C. is an employee of EP Solutions. K.-H.K. is a consultant to EP Solutions.

Funding

This study was in part funded by a grant from the Russian Science Foundation, Project # 14-15-01097, "Noninvasive Electrocardiographic Imaging for Diagnostics and Catheter Ablation Guidance of Atrial Fibrillation and Atrial Flutter: a Feasibility Study". Funding to pay the Open Access publication charges for this article was provided by EP Solutions.

References

1. Oster HS, Taccardi B, Lux RL, Ershler PR, Rudy Y. Noninvasive electrocardiographic imaging: reconstruction of epicardial potentials, electrograms, and isochrones and localization of single and multiple electrocardiac events. *Circulation* 1997;**96**:1012–24.
2. Burnes JE, Taccardi B, Rudy Y. A noninvasive imaging modality for cardiac arrhythmias. *Circulation* 2000;**102**:2152–8.
3. Blomström Lundqvist C, Auricchio A, Brugada J, Boriani G, Bremerich J, Cabrera JA *et al.* The use of imaging for electrophysiological and devices procedures: a report from the first European Heart Rhythm Association Policy Conference, jointly organized with the European Association of Cardiovascular Imaging (EACVI), the Council of Cardiovascular Imaging and the European Society of Cardiac Radiology. *Europace* 2013;**15**:927–36.
4. Shah AJ, Hocini M, Xhaet O, Pascale P, Roten L, Wilton SB *et al.* Validation of novel 3-dimensional electrocardiographic mapping of atrial tachycardias by invasive mapping and ablation: a multicenter study. *J Am Coll Cardiol* 2013;**62**:889–97.
5. Wang Y, Schuessler RB, Damiano RJ, Woodard PK, Rudy Y. Noninvasive electrocardiographic imaging (ECGI) of scar-related atypical atrial flutter. *Heart Rhythm* 2007;**4**:1565–7.
6. Intini A, Goldstein RN, Jia P, Ramanathan C, Ryu K, Giannattasio B *et al.* Electrocardiographic imaging (ECGI), a novel diagnostic modality used for mapping of focal left ventricular tachycardia in a young athlete. *Heart Rhythm* 2005;**2**:1250–2.
7. Jia P, Ramanathan C, Ghanem RN, Ryu K, Varma N, Rudy Y. Electrocardiographic imaging of cardiac resynchronization therapy in heart failure: observation of variable electrophysiologic responses. *Heart Rhythm* 2006;**3**:296–310.
8. Cuculich PS, Wang Y, Lindsay BD, Faddis MN, Schuessler RB, Damiano RJ Jr *et al.* Noninvasive characterization of epicardial activation in humans with diverse atrial fibrillation patterns. *Circulation* 2010;**122**:1364–72.
9. Haissaguerre M, Hocini M, Shah AJ, Derval N, Sacher F, Jais P *et al.* Noninvasive panoramic mapping of human atrial fibrillation mechanisms: a feasibility report. *J. Cardiovasc Electrophysiol* 2013;**24**:711–7.
10. Bokeriia LA, Revishvili A, Kalinin AV, Kalinin VV, Liadzhina OA, Fetisova EA. Hardware-software system for noninvasive electrocardiographic examination of heart based on inverse problem of electrocardiography. *Meditsinskaia tekhnika* 2008;**6**:1–7.
11. Denisov AM, Zakharov EV, Kalinin AV, Kalinin VV. Numerical solution of an inverse electrocardiography problem for a medium with piecewise constant electrical conductivity. *Comput Math Math Phys* 2010;**50**:1172–7.
12. Kalinin AV. Iterative algorithm for the inverse problem of electrocardiography in a medium with piecewise-constant electrical conductivity. *Comput Math Math Phys* 2011;**22**:30–4.
13. Tilg B, Fischer G, Modre R, Hanser F, Messnarz B, Schocke M *et al.* Model-based imaging of cardiac electrical excitation in humans. *IEEE Trans Med Imaging* 2002;**21**:1031–9.
14. Modre R, Tilg B, Fischer G, Hanser F, Messnarz B, Seger M *et al.* Atrial noninvasive activation mapping of paced rhythm data. *J Cardiovasc Electrophysiol* 2003;**14**:712–9.
15. Lorensen WE, Cline HE. Marching cubes: a high resolution 3D surface construction algorithm. *SIGGRAPH Comput Graph* 1987;**21**:163–9.
16. Shephard MS, Georges MK. Automatic three-dimensional mesh generation by the finite octree technique. *Int J Numer Meth Eng* 1991;**32**:709–749.
17. Lo SH. Volume discretization into tetrahedra—II. 3D triangulation by advancing front approach. *Comput Struct* 1991;**39**:501–11.